HHS Public Access

Author manuscript

Mol Imaging Biol. Author manuscript; available in PMC 2021 October 01.

Published in final edited form as:

Mol Imaging Biol. 2020 October ; 22(5): 1353–1361. doi:10.1007/s11307-020-01513-9.

PET detection of cerebral necrosis using an infarct-avid agent 2-deoxy-2-[^{18}F]fluoro-D-glucaric acid (FGA) in a mouse model of the brain stroke

Hailey Houson, BS[1], **Alexander Mdzinarishvili, PhD**[1], **Hariprasad Gali, PhD**[1], **Evgeny Sidorov, MD**[2], **Vibhudutta Awasthi, PhD**[1,3,*]

[1]Department of Pharmaceutical Sciences, University of Oklahoma Health Sciences Center, 1110 N. Stonewall Avenue, Oklahoma City, OK 73117;

[2]Department of Neurology, University of Oklahoma Health Sciences Center, 1110 N. Stonewall Avenue, Oklahoma City, OK 73117;

[3]Hexakit, Inc., 2401 Cheval Pointe Dr. Edmond, OK 73034

Abstract

Purpose—Ischemic stroke is a leading cause of disability worldwide. The volume of necrotic core in affected tissue plays a major role in selecting stroke patients for thrombolytic therapy or endovascular thrombectomy. In this study we investigated a recently reported PET agent 2-deoxy-2-[^{18}F]fluoro-D-glucaric acid (FGA) to determine necrotic core in a model of transient middle cerebral artery occlusion (t-MCAO) in mice.

Procedures—The radiopharmaceutical, FGA, was synthesized by controlled, rapid, and quantitative oxidation of clinical doses of 2-deoxy-2-[^{18}F]fluoro-D-glucose (FDG) in a one-step reaction using a premade kit. Brain stroke was induced in the left cerebral hemisphere of CD-1 mice by occluding the middle cerebral artery for 1 h, and then allowing reperfusion by removing the occlusion. One day post ictus, perfusion SPECT was performed with 99mTc-lableled hexamethylpropyleneamine oxime (HMPAO), followed by PET acquisition with FGA. Plasma and brain tissue homogenates were assayed for markers of inflammation and neurotrophins.

Results—The kit-based synthesis was able to convert up to 2.2 GBq of FDG into FGA within 5 min. PET images showed 375% more accumulation of FGA in ipsilateral hemisphere than in the contralateral hemisphere. SPECT images showed that ipsilateral HMPAO accumulation was reduced to 55% of normal levels; there was significant negative correlation between ipsilateral accumulation of FGA and HMAPO ($p < 0.05$). FGA accumulation in stroke also correlated with

*Corresponding author: Vibhudutta Awasthi, Ph.D., Department of Pharmaceutical Sciences, 1110 N. Stonewall Avenue, CPB 309, Oklahoma City, OK 73117, USA, Phone: 405-271-6593, vawasthi@ouhsc.edu.

Conflict of Interest Statement

VA is partly employed by Hexakit, Inc. and is its owner.

IL-6 levels in the ipsilateral hemisphere. There was no change in IL-6 or TNF-α in the plasma of stroke mice.

Conclusions—Accumulation of FGA correlated well with the perfusion defect and inflammatory injury. As a PET agent, FGA has potential to image infarcted core in the brain stroke injury with high sensitivity, resolution, and specificity.

Keywords

Brain stroke; infarct; ischemia core; fluorodeoxyglucaric acid; positron emission tomography

Introduction

Stroke is a cerebrovascular disease associated with sudden loss of neurologic function. It affects more than 800,000 individuals every year [1]. More than 80% of brain strokes are ischemic, caused by interruption of blood supply to the brain from thrombotic or embolic cerebrovascular occlusion, and the rest are categorized as hemorrhagic [2]. Ischemic stroke is a time-sensitive event requiring immediate recognition and intervention to salvage viable tissue which is threatened by hypoperfusion. A failed or delayed diagnosis of stroke is a missed opportunity for prompt treatment to alter an otherwise poor prognosis. It is believed that mortality and morbidity associated with stroke can be significantly reduced if location and extent of injury are divulged early after symptoms emerge [8, 9]. Depending on the regional perfusion thresholds, ischemic stroke comprises of 3 regions- olegemic (above 18–20 ml/100 g/min, but below normal 50–60 ml/100 g/min), penumbra (~10–18 ml/100 g/min), and infarct (less than 10 ml/100 g/min). Olegemic tissue shows no functional impairment, but penumbra transitions into infarction within 6 h post ictus, if left unattended [3]. A large infarct characterized by widespread necrosis predicts poor patient outcome and correlates with an increased risk of cerebral hemorrhage upon reperfusion [4–5]. Given the dynamic evolution of ischemic penumbra into infarct, accurate and rapid delineation of these regions is critical for clinical decision to salvage metabolically viable tissue.

In the context of urgency in diagnostic evaluation of brain stroke, it is noteworthy that the efficacy of tissue plasminogen activator (t-PA) therapy in stroke patients is limited to the first 4.5 h post ictus [6–7]. Selection of patients for surgical embolectomy is also dependent on diagnostic information about the volume of stroke core which is an area of irreversible brain damage [8–9]. Diffusion magnetic resonance imaging (MRI) is the gold standard for evaluation of stroke core, but it involves a lengthy procedure. Therefore, stroke core is commonly estimated from perfusion computed tomography (CTP). However, CTP is very operator-dependent and requires infusion of iodine contrast. Moreover, MR imaging with or without contrast in the acute phase may be obscured by an underlying neoplastic lesion, vascular mass or stroke-associated microhemorrhages and hematomas [10].

In this article we describe an application of positron emission tomography (PET) infarct-avid agent 2-deoxy-2-[^{18}F]fluoro-D-glucaric acid (FGA) for determining necrotic areas in ischemic stroke in a mouse model. Our lab has previously shown that FGA can delineate myocardial necrosis in a chemically induced myocardial infarction model [11]. We hypothesized that FGA will accumulate in cerebral infarct inversely to perfusion. Agents

that target necrosis typically have an intracellular molecular target, but are unable to cross intact cell membranes [12–13]. During necrosis, disruption of the cell membrane allows these agents to bind to their targets. Putatively, radiolabeled glucaric acid is believed to bind to positively charged histone proteins [11, 14].

Materials and Methods

Synthesis of FGA and quality control

We synthesized FGA from commercially available 2-deoxy-2-[^{18}F]fluoro-D-glucose (FDG). The pre-formulation data leading up to a kit has been published elsewhere [11]. A typical kit vial contained a lyophilized mixture of 0.8 mg of 2,2,6,6-tetramethyl-1-piperidinyloxy or TEMPO (Sigma-Aldrich, St. Louis, MO), 8 mg of sodium bromide (NaBr, Mallinckrodt, Paris, Kentucky, USA), and 24 mg sodium bicarbonate ($NaHCO_3$, Sigma-Aldrich). For conversion of FDG into FGA, FDG was introduced into the vial in presence of 20 μL NaOCl (14% available chlorine, Alfa Aesar, Tewksbury, MA). After 5 min, the reaction was stopped and the mixture was neutralized by 1.5 mL of 0.2 M hydrochloric acid (HCl). The resultant product was drawn into a syringe for injection via a 0.2 μm syringe filter. The presence of FGA and FDG in the final preparation was monitored by thin-layered chromatography (TLC) as described elsewhere [11].

Mouse model of transient middle cerebral artery occlusion (t-MCAO)

Animal experiments were conducted in accordance with NIH animal care and use guidelines and were approved by the IACUC at the University of Oklahoma Health Sciences Center. Focal brain ischemia by t-MCAO was induced in mice as described in detail previously [15]. Male CD-1 mice (2–3 mo; 25–30 g) were obtained from Charles River lab (San Diego, CA) and acclimatized for at least 3 days. Mice were anesthetized with 1.5% isoflurane in a stream of oxygen during surgery. Middle cerebral artery was occluded by inserting a 15 mm monofilament 6–0 nylon suture with tip diameter of 0.2–0.3mm. The monofilament was secured in place and the skin incision was closed by ligature. After 1 h, the monofilament was withdrawn to allow tissue reperfusion. Sham-operated mice underwent surgery without occlusion and reperfusion steps.

Perfusion imaging by single photon emission tomography (SPECT)

Perfusion deficit created by arterial occlusion was detected by SPECT using ^{99m}Tc-labeled hexamethylpropyleneamine oxime (HMPAO). Approximately 2.5 mCi (92.5 MBq) of HMPAO in 150 μL volume was injected via tail vein of a mouse under isoflurane anesthesia. At 1 h post injection, mice were re-anesthetized and placed in the NanoSPECT machine (Bioscan, Washington DC). Helical SPECT of the brain was acquired in 24 frames of 45 sec each. After SPECT imaging, the mice were immediately set up for PET imaging.

Infarct imaging by PET and uptake of FGA in ipsilateral cerebral hemisphere

Isoflurane-anesthetized mice were injected with 92.5 MBq (2.5 mCi) of FGA via a tail vein (150–200 μL). At 1 and 2 h post-injection, list-mode data acquisition was performed for 10 min using a PET-CT machine (Gamma Medica Ideas, Northridge, CA). After live animal imaging was accomplished, the mice were euthanized and their skull and brain were

removed for *ex vivo* PET acquisition for 10 min. In a separate cohort, mice were injected with 250 μCi (9.2 MBq) of FGA (200 μL) for counting of tissue-associated radioactivity in ipsilateral versus contralateral cerebral hemispheres. Mice were euthanized 1 h after FGA injection and brain was carefully removed. Right and left hemispheres were separated at the midline, placed in separate cryo-vials, weighed, and counted in a well counter (Ludlum-2200, Sweetwater, TX). Tissue-associated counts were background subtracted and radioactivity was decay-corrected to injection time.

Histology

Approximately 24 h post-ictus, mice were deeply anaesthetized with isoflurane (4%) and euthanized by decapitation. The brain was quickly removed and sectioned coronally into slices of 1 mm thickness. Slices were incubated in a 1% solution of 2,3,5-triphenyltetrazolium chloride (TTC) in phosphate-buffered saline at 37 °C (in water bath) for 20 min and then fixed by immersion in 4% buffered formaldehyde solution. Images of TTC-stained slices were acquired by digital camera, and areas of both hemispheres and the infarcted regions were quantified using Amira image analysis software (Fei-Thermo Fisher, Hillsboro, Oregon). We measured the areas of brain edema by increase in area in the ipsilateral (ischemic) hemisphere compared to the contralateral (non-ischemic) hemisphere [16].

Cytokine (IL-6 and TNF-α) enzyme-linked immunoassay (ELISA)

IL-6 and TNF-α were determined in brain tissue and plasma samples using ELISA kits and following the manufacturer's recommendations (BioLegend, San Diego, CA). To prepare tissue homogenate, brain tissue was homogenized in PBS containing phosphatase arrest I and mammalian protease arrest (G-Biosciences, St Louis, MO). Protein concentration in tissue homogenate was determined by Pierce bicinchoninic acid assay (Thermo Fisher, Hillsboro, Oregon). Samples were run in duplicate and normalized to protein concentration. Plasma samples were run undiluted for TNF-α and at a 5-fold dilution for IL-6.

Brain-derived nerve factor (BDNF) and nerve growth factor (NGF)-β

Mouse BDNF and NGF-β ELISA kits were purchased from Boster Biochem (Pleasanton, CA). Tissue samples were processed as described above for IL-6 and TNF-α assays.

Data analysis

Data are presented as the mean ± standard error of mean. Two group comparisons were done with a Student's unpaired t-test. P values in figures are expressed as $p < 0.05$ (*), $p < 0.01$ (**), $p < 0.001$ (***), or $p < 0.0001$ (****). Correlation was assessed with linear regression and R^2 goodness of fit. SPECT and PET images were analyzed by region of interest (ROI) analyses and tracer accumulation was compared in matched regions of SPECT and PET images. Accumulation in each section was measured with the material statistics application of Amira 6 software (Thermo Fisher Scientific, Waltham, MA).

Results

Synthesis of FGA from kit-enabled oxidation of FDG

Synthesis of FGA was accomplished in a quantitative manner from rapid oxidation of FDG in an optimized kit. Synthesis was routinely completed within 5 min of initiation and no untoward reaction side products were observed.

Mouse model of t-MCAO

Figure 1A shows the timeline of surgery and imaging. Ischemic duration of 1 h was followed by approximately 16 h of reperfusion. Afterwards, the mice were subjected to SPECT and PET imaging sessions. Figure 1B shows typical TTC-stained slices of brain from sham and stroke mice. Necrosis is known to set in within minutes of cerebral vessel occlusion because the viability of brain is entirely dependent on a continuous blood supply. We observed large areas of necrotic tissue and significant brain edema in the ipsilateral hemisphere of mice with t-MCAO. Viable tissue with intact mitochondrial function was stained dark red by TTC, whereas infarcted tissue remained unstained. Digital pictures of TTC-stained slices were used to measure brain edema (swelling) associated with stroke. Edema was quantified as the difference in area of the ipsilateral hemisphere and that of the contralateral hemisphere on slice basis. As shown in Figure 1C, compared to the contralateral area, ipsilateral hemisphere showed a significant increase.

Inflammatory cytokines and neurotrophins

Inflammatory cytokines IL-6 and TNF-α were investigated in brain tissue and plasma samples obtained from sham-operated and stroke mice (Figure 2). IL-6 concentration was approximately 30 pg/mg in brain tissue from sham mice as compared to 2,500 pg/mg in ipsilateral tissue from stroke mice (Figure 2A). Tissue levels of TNF-α appeared to increase due to stroke, but the increase was not statistically significant (Figure 2B). In plasma samples, there was no significant alteration in IL-6 or TNF-α between the stroke and sham group (Figure 2C and 2D, respectively).

Levels of neurotrophins BDNF and NGF-β were investigated in the ipsilateral hemispheres collected 24 h post-stroke. We observed a significant decrease in levels of BDNF in stroke brain tissue as compared to that in sham brain tissue (Figure 3A). This observation of a decrease in BDNF concentration in the ipsilateral brain tissue is in congruence with other reports [17–18]. However, plasma levels of BDNF in pooled plasma samples from our model was undetectable (data not shown). Moreover, there was no change in brain levels of NGF-β (Figure 3B).

Accumulation of FGA in stroke

We determined radioactivity counts (counts per min or CPM) in brains excised from stroke and sham mice. As expected, the ipsilateral to contralateral (I/C) counts ratio in sham operated mice was close to 1, meaning that the ipsilateral and contralateral hemispheres accumulated the same amount of radioactivity (Figure 4A). On the other hand, in stroke mice the ipsilateral hemisphere accumulated almost twice the FGA as compared to the contralateral hemisphere. When FGA accumulation ratio (ipsilateral/contralateral) was

compared with ipsilateral brain tissue IL-6 levels, we found a significant correlation between the two (Figure 4B).

Perfusion imaging with HMPAO/SPECT versus FGA/PET imaging in stroke mice

We found that there was a generalized lack of accumulation of HMPAO in the ipsilateral hemisphere as compared to the contralateral hemisphere (Figure 5A). It is noteworthy that the area of perfusion defect depicted by HMPAO/SPECT was larger than the histological infarct size shown by TTC staining. Image analysis showed that HMPAO accumulation in the ipsilateral hemisphere decreased to 45% of normal levels- 5,950 CPM/mm^3 in normal brain tissue compared to 3,270 CPM/mm^3 in ipsilateral tissue (Figure 5B). In contrast to the HMPAO/SPECT perfusion images, FGA/PET images showed accumulation of FGA in the stroke region of the ipsilateral hemisphere. Initial *in vivo* FGA/PET images were difficult to interpret due to the small volume of injury surrounded by non-specific accumulation of FGA in the nasopharyngeal region. From *ex vivo* imaging, we found that there was significantly more accumulation of FGA in the ipsilateral hemisphere as compared to the contralateral hemisphere (Figure 5C). Digital analysis of brain PET images also showed an increase in CPM/mm^3 in ipsilateral tissue; ipsilateral tissue accumulated 34.2 ± 9.2 CPM/mm^3 and the contralateral tissue accumulated 9.0 ± 6.7 CPM/mm^3 (Figure 5D). This region of increased FGA accumulation correlated very well with the infarct region depicted by TTC staining (Figure 5E). When FGA accumulation was compared with HMPAO accumulation in the same spatial plane, we found that the two were negatively correlated ($p = 0.0054$), indicating that areas with poor perfusion and low HMPAO accumulation, accrued significant amounts of FGA (Figure 5F).

Following the above-described comparison between HMPAO/SPECT and FGA/PET, we recruited another set of three mice with t-MCAO for *in vivo* PET within 3 h of stroke surgery which is clinically more relevant. Images were acquired 1–2 h after injecting 7 – 8 MBq FGA. As shown in Figure 6, FGA/PET clearly delineated ipsilateral hemisphere from the contralateral hemisphere.

Discussion

Results of our study indicate that FGA/PET allows accurate imaging of necrotic tissue within the ischemic area of the brain, directly visualizing the stroke core. Direct visualization of necrotic core is very different from conventional practice of CTP in which the stroke core is estimated by the volume of iodine contrast delivered to infarcted brain tissue. In CTP studies, cerebral blood volume (CBV) of < 2 mL/100 g is thought to correlate with the infarcted core [19]; however, the accuracy of CTP often suffers from incorrect selection of arterial inflow point, venous outflow point, and suboptimal timing of contrast infusion [20]. One study showed that observer variability for CBV from CTP study was 11–18% [21]. In addition, CTP cannot identify small infarcts and has poor sensitivity for infra-tentorial strokes [22]. In contrast, FGA/PET can potentially detect small infarcts with high precision as shown by the results in this mouse model of ischemic stroke. Accurate determination of the stroke core follows current trends in clinical acute ischemic stroke research. Recently published DAWN and DEFUSE-3 trials showed that endovascular

thrombectomy for acute ischemic stroke patients may be performed even 24 h after onset of symptoms. Both studies put ischemic core volume as a major selection criteria for endovascular intervention: 70 mL at 16 h and 50 ml at 24 h [8–9]. A better method for ischemic core delineation should improve clinical decision making [23]. FGA/PET may also provide certain advantages when compared to MRI. Diffusion-perfusion MRI images tend to overestimate ischemic penumbra due to inclusion of oligemic tissue [24–26]. Additionally, there is lack of consensus on thresholds employed for delineating diffusion-perfusion deficits in MRI. These issues were highlighted in a study comparing MRI data with the data obtained from PET using an ischemia-specific agent, [^{18}F]fluoromisonidazole (FMISO). FMISO accumulates in ischemic, but not necrotic tissue, while lesions in diffusion-weighted MR images are known to include necrotic core and portions of ischemic penumbra [25, 27].

Application of PET imaging in the management of stroke and occlusive cerebrovascular diseases is mostly related to quantitation of cerebral blood flow (CBF), CBV, cerebral metabolic rate of oxygen, and cerebral metabolic rate of glucose [28]. In these studies, ^{18}F ($T_{1/2}$ = 110 min), very short-lived ^{15}O ($T_{1/2}$ = 2 min) and ^{11}C ($T_{1/2}$ = 20 min) imaging agents are employed. For example, CBF determination with [^{15}O]H_2O/PET is widely recommended for moyamoya- a chronic stenoocclusive vasculopathy affecting the terminal internal carotid arteries [29]. Although information about region-specific metabolism derived from PET studies is unmatched in value, its diagnostic utility in stroke is limited to CBF evaluations due to the technical logistics and complex data analyses algorithms [28]. Even then, ischemia imaging with FMISO/PET has shown close correlation with patient outcome post-stroke by quantifying penumbra [30–31]. However, FMISO only accumulates in ischemic tissue and is excluded by necrotic core (infarct). Since the growth of the necrotic region is a dynamic process, the evolution of the ischemic area into a necrotic tissue can only be assessed by an infarct-avid agent. It is believed that infarct-avid agents can detect infarction as soon as 30 min after blood flow is blocked [32], facilitating rapid patient assessment and evidence-based treatment. FGA/PET has a potential to fill this unmet medical need of infarct core quantitation [33]. Another radiolabeled glucaric acid product, ^{99m}Tc-labeled glucarate, has also been previously investigated for SPECT in a rat model of MCAO [34] as well as in myocardial infarct by several groups with some success [35–37]. Like ^{99m}Tc-labeled glucarate, FGA targets early cellular changes that occur in infarction, which enables it to localize an infarct, even in patients with subtle symptoms or metabolic perturbations [11, 14]. In addition, FGA undergoes rapid clearance and does not accumulate in normal brain which would otherwise create imaging artifacts [11].

Among various easily assayable plasma markers of stroke severity, IL-6 is considered as an early clinical marker [38–39]. A previous animal study also reported elevated plasma levels of inflammatory markers (IL-6 and TNF-α) 24 h post ictus [40]. However, plasma levels of these inflammatory markers were not altered in our model by localized brain injury; at the same time, brain tissue levels of IL-6 and TNF-α were increased which is consistent with another published report [41]. It is possible that the severity of injury was not sufficient to cause systemic inflammatory response in our model. Based on the observation that brain tissue IL-6 levels and FGA accumulation in injured tissue correlated very well (Figure 4b), FGA/PET can have utility in assessment of the extent of tissue damage using non-invasive imaging.

Like perfusion data from CTP for discrimination of penumbra from infarcted tissue [42–43], perfusion information from HMPAO/SPECT has also been employed to determine brain tissue salvageability [44–45]. Perfusion parameters detected by HMPAO/SPECT have been shown to correlate very well with peak and mean transit time parameters determined by CTP [46]. It can also determine cerebrovascular reserve in stroke patients [47]. In rat models, HMPAO/SPECT showed reduced perfusion as soon as 2 h [48] and as late as 24 h post-stroke [49]. In a coagulated model of permanent occlusive stroke, Ceulemans et al. observed a 20% decrease in HMPAO accumulation 24 h post-stroke [50]. In our model, we observed a 45% decrease in ipsilateral accumulation of HMPAO as compared to contralateral tissue 24 h after stroke. Compared to HMPAO, ipsilateral accumulation of FGA was 375% more than that in the contralateral hemisphere. FGA accrual in the ipsilateral hemisphere strongly correlated with a corresponding reduction in HMPAO accumulation.

Conclusions

Development of an imaging technique that can positively localize infarcted tissue in the brain stroke with high sensitivity and specificity improves the diagnostic accuracy, which can allow better selection of patients for endovascular intervention. In this study, we demonstrated the feasibility of FGA/PET in a mouse model of t-MCAO stroke. FGA accumulation strongly correlated with inflammatory marker IL-6 in brain tissue as well as with perfusion indicator HMPAO. Clear delineation of infarct by FGA/PET is expected to complement other imaging modalities in identifying patients who would benefit from revascularization, and exclude those at a high risk of hemorrhage. This role of FGA/PET is likely to expand upon further testing and as more data become available.

Acknowledgements

This study was partly funded by 1R41HL140919-01A1 STTR grant to Hexakit, Inc. Technical assistance from Ms. Andria Hedrick is acknowledged.

References

1. Benjamin EJ, Blaha MJ, Chiuve SE, et al. (2017) Heart Disease and Stroke Statistics-2017 Update: A Report From the American Heart Association. Circulation 135:e146–e603. [PubMed: 28122885]
2. Donnan GA, Fisher M, Macleod M, Davis SM (2008) Stroke. Lancet 371:1612–1623. [PubMed: 18468545]
3. Read SJ, Hirano T, Abbott DF, et al. (1998) Identifying hypoxic tissue after acute ischemic stroke using PET and 18F-fluoromisonidazole. Neurology 51:1617–1621. [PubMed: 9855512]
4. Castro P, Azevedo E, Serrador J, Rocha I, Sorond F (2017) Hemorrhagic transformation and cerebral edema in acute ischemic stroke: Link to cerebral autoregulation. Journal of the neurological sciences 372:256–261. [PubMed: 28017224]
5. (1997) Intracerebral hemorrhage after intravenous t-PA therapy for ischemic stroke. The NINDS t-PA Stroke Study Group. Stroke 28:2109–2118. [PubMed: 9368550]
6. Chang P, Prabhakaran S (2017) Recent advances in the management of acute ischemic stroke. F1000Research 6.
7. Powers WJ, Rabinstein AA, Ackerson T, et al. (2018) 2018 Guidelines for the Early Management of Patients With Acute Ischemic Stroke: A Guideline for Healthcare Professionals From the American Heart Association/American Stroke Association. Stroke 49:e46–e110. [PubMed: 29367334]
8. Albers GW, Marks MP, Kemp S, et al. (2018) Thrombectomy for Stroke at 6 to 16 Hours with Selection by Perfusion Imaging. N Engl J Med 378:708–718. [PubMed: 29364767]

9. Nogueira RG, Jadhav AP, Haussen DC, et al. (2018) Thrombectomy 6 to 24 Hours after Stroke with a Mismatch between Deficit and Infarct. N Engl J Med 378:11–21. [PubMed: 29129157]
10. Wintermark M, Sanelli PC, Albers GW, et al. (2013) Imaging recommendations for acute stroke and transient ischemic attack patients: a joint statement by the American Society of Neuroradiology, the American College of Radiology and the Society of NeuroInterventional Surgery. J Am Coll Radiol 10:828–832. [PubMed: 23948676]
11. Houson HA, Nkepang GN, Hedrick AF, Awasthi V (2018) Imaging of isoproterenol-induced myocardial injury with (18)F labeled fluoroglucaric acid in a rat model. Nuclear medicine and biology 59:9–15. [PubMed: 29413753]
12. Taillefer R, Boucher L, Lambert R, Gregoire J, Phaneuf DC, Sikorsa H (1995) Technetium-99m antimyosin antibody (3–48) myocardial imaging: human biodistribution, safety and clinical results in detection of acute myocardial infarction. European journal of nuclear medicine 22:453–464. [PubMed: 7641754]
13. Bokhari S, Castano A, Pozniakoff T, Deslisle S, Latif F, Maurer MS (2013) (99m)Tc-pyrophosphate scintigraphy for differentiating light-chain cardiac amyloidosis from the transthyretin-related familial and senile cardiac amyloidoses. Circulation Cardiovascular imaging 6:195–201. [PubMed: 23400849]
14. Khaw BA, Silva JD, Petrov A, Hartner W (2002) Indium 111 antimyosin and Tc-99m glucaric acid for noninvasive identification of oncotic and apoptotic myocardial necrosis. Journal of nuclear cardiology : official publication of the American Society of Nuclear Cardiology 9:471–481. [PubMed: 12360127]
15. Mdzinarishvili A, Geldenhuys WJ, Abbruscato TJ, Bickel U, Klein J, Van der Schyf CJ (2005) NGP1–01, a lipophilic polycyclic cage amine, is neuroprotective in focal ischemia. Neuroscience letters 383:49–53. [PubMed: 15936510]
16. Sydserff SG, Green AR, Cross AJ (1996) The effect of oedema and tissue swelling on the measurement of neuroprotection; a study using chlormethiazole and permanent middle cerebral artery occlusion in rats. Neurodegeneration : a journal for neurodegenerative disorders, neuroprotection, and neuroregeneration 5:81–85.
17. Harada S, Yamazaki Y, Tokuyama S (2013) Orexin-A suppresses postischemic glucose intolerance and neuronal damage through hypothalamic brain-derived neurotrophic factor. The Journal of pharmacology and experimental therapeutics 344:276–285. [PubMed: 23117790]
18. Shu X, Zhang Y, Xu H, Kang K, Cai D (2013) Brain-derived neurotrophic factor inhibits glucose intolerance after cerebral ischemia. Neural regeneration research 8:2370–2378. [PubMed: 25206547]
19. Tan JC, Dillon WP, Liu S, Adler F, Smith WS, Wintermark M (2007) Systematic comparison of perfusion-CT and CT-angiography in acute stroke patients. Ann Neurol 61:533–543. [PubMed: 17431875]
20. Oei MTH, Meijer FJA, van der Woude WJ, et al. (2017) Interleaving cerebral CT perfusion with neck CT angiography part I. Proof of concept and accuracy of cerebral perfusion values. Eur Radiol 27:2649–2656. [PubMed: 27718078]
21. Waaijer A, van Leeuwen MS, van Osch MJ, et al. (2007) Changes in cerebral perfusion after revascularization of symptomatic carotid artery stenosis: CT measurement. Radiology 245:541–548. [PubMed: 17848682]
22. Bollwein C, Plate A, Sommer WH, et al. (2016) Diagnostic accuracy of whole-brain CT perfusion in the detection of acute infratentorial infarctions. Neuroradiology 58:1077–1085. [PubMed: 27651328]
23. Lee DH, Kang DW, Ahn JS, Choi CG, Kim SJ, Suh DC (2005) Imaging of the ischemic penumbra in acute stroke. Korean journal of radiology 6:64–74. [PubMed: 15968144]
24. Heiss WD, Sobesky J, Hesselmann V (2004) Identifying thresholds for penumbra and irreversible tissue damage. Stroke 35:2671–2674. [PubMed: 15459433]
25. Guadagno JV, Warburton EA, Aigbirhio FI, et al. (2004) Does the acute diffusion-weighted imaging lesion represent penumbra as well as core? A combined quantitative PET/MRI voxel-based study. Journal of cerebral blood flow and metabolism : official journal of the International Society of Cerebral Blood Flow and Metabolism 24:1249–1254.

26. Heiss WD, Zaro Weber O (2017) Validation of MRI Determination of the Penumbra by PET Measurements in Ischemic Stroke. Journal of nuclear medicine : official publication, Society of Nuclear Medicine 58:187–193.
27. Lee GH, Kim JS, Oh SJ, Kang DW, Kwon SU (2015) (18)F-fluoromisonidazole (FMISO) Positron Emission Tomography (PET) Predicts Early Infarct Growth in Patients with Acute Ischemic Stroke. Journal of neuroimaging : official journal of the American Society of Neuroimaging 25:652–655. [PubMed: 25311732]
28. Heiss WD (2014) Radionuclide imaging in ischemic stroke. Journal of nuclear medicine : official publication, Society of Nuclear Medicine 55:1831–1841.
29. Lee M, Zaharchuk G, Guzman R, Achrol A, Bell-Stephens T, Steinberg GK (2009) Quantitative hemodynamic studies in moyamoya disease: a review. Neurosurg Focus 26:E5.
30. Read SJ, Hirano T, Abbott DF, et al. (2000) The fate of hypoxic tissue on 18F-fluoromisonidazole positron emission tomography after ischemic stroke. Ann Neurol 48:228–235. [PubMed: 10939574]
31. Markus R, Reutens DC, Kazui S, et al. (2004) Hypoxic tissue in ischaemic stroke: persistence and clinical consequences of spontaneous survival. Brain : a journal of neurology 127:1427–1436. [PubMed: 15130953]
32. Narula J, Petrov A, Pak KY, Khaw B-A (1995) 962–122 Very Early Noninvasive Imaging of Acute Myocardial Infarcts with Tc-99m-Glucarate. J Am Coll Cardiol 25:218A–218A. [PubMed: 7798505]
33. Morgan CD, Stephens M, Zuckerman SL, et al. (2015) Physiologic imaging in acute stroke: Patient selection. Interventional neuroradiology : journal of peritherapeutic neuroradiology, surgical procedures and related neurosciences 21:499–510.
34. Yaoita H, Uehara T, Brownell AL, et al. (1991) Localization of technetium-99m-glucarate in zones of acute cerebral injury. Journal of nuclear medicine : official publication, Society of Nuclear Medicine 32:272–278.
35. Khaw B-A, Nakazawa A, O'Donnell S, Pak K-Y, Narula J (1997) Avidity of technetium 99m glucarate for the necrotic myocardium: In vivo and in vitro assessment. Journal of Nuclear Cardiology 4:283–290. [PubMed: 9278874]
36. Gerson MC, McGoron AJ (1997) Technetium 99m glucarate: what will be its clinical role? Journal of nuclear cardiology : official publication of the American Society of Nuclear Cardiology 4:336–340. [PubMed: 9278881]
37. Choudhury PS, Savio E, Solanki KK, et al. (2012) (99m)Tc glucarate as a potential radiopharmaceutical agent for assessment of tumor viability: from bench to the bed side. World journal of nuclear medicine 11:47–56. [PubMed: 23372437]
38. Waje-Andreassen U, Krakenes J, Ulvestad E, et al. (2005) IL-6: an early marker for outcome in acute ischemic stroke. Acta Neurol Scand 111:360–365. [PubMed: 15876336]
39. Gandolfi M, Smania N, Vella A, Picelli A, Chirumbolo S (2017) Assessed and Emerging Biomarkers in Stroke and Training-Mediated Stroke Recovery: State of the Art. Neural Plast 2017:1389475. [PubMed: 28373915]
40. Li P, Mao L, Zhou G, et al. (2013) Adoptive regulatory T-cell therapy preserves systemic immune homeostasis after cerebral ischemia. Stroke 44:3509–3515. [PubMed: 24092548]
41. Sieber MW, Claus RA, Witte OW, Frahm C (2011) Attenuated inflammatory response in aged mice brains following stroke. PloS one 6:e26288. [PubMed: 22028848]
42. Lui YW, Tang ER, Allmendinger AM, Spektor V (2010) Evaluation of CT perfusion in the setting of cerebral ischemia: patterns and pitfalls. AJNR Am J Neuroradiol 31:1552–1563. [PubMed: 20190208]
43. Knoepfli AS, Sekoranja L, Bonvin C, et al. (2009) Evaluation of perfusion CT and TIBI grade in acute stroke for predicting thrombolysis benefit and clinical outcome. J Neuroradiol 36:131–137. [PubMed: 19062093]
44. Alexandrov AV, Black SE, Ehrlich LE, et al. (1996) Simple visual analysis of brain perfusion on HMPAO SPECT predicts early outcome in acute stroke. Stroke 27:1537–1542. [PubMed: 8784126]

45. Umemura A, Suzuka T, Yamada K (2000) Quantitative measurement of cerebral blood flow by (99m)Tc-HMPAO SPECT in acute ischaemic stroke: usefulness in determining therapeutic options. Journal of neurology, neurosurgery, and psychiatry 69:472–478.

46. Eicker SO, Turowski B, Heiroth HJ, Steiger HJ, Hanggi D (2011) A comparative study of perfusion CT and 99m Tc-HMPAO SPECT measurement to assess cerebrovascular reserve capacity in patients with internal carotid artery occlusion. European journal of medical research 16:484–490. [PubMed: 22027641]

47. Lewis DH, Toney LK, Baron JC (2012) Nuclear medicine in cerebrovascular disease. Seminars in nuclear medicine 42:387–405. [PubMed: 23026361]

48. Szigeti K, Horvath I, Veres DS, et al. (2015) A novel SPECT-based approach reveals early mechanisms of central and peripheral inflammation after cerebral ischemia. Journal of cerebral blood flow and metabolism : official journal of the International Society of Cerebral Blood Flow and Metabolism 35:1921–1929.

49. Martin A, Mace E, Boisgard R, et al. (2012) Imaging of perfusion, angiogenesis, and tissue elasticity after stroke. Journal of cerebral blood flow and metabolism : official journal of the International Society of Cerebral Blood Flow and Metabolism 32:1496–1507.

50. Ceulemans AG, Hernot S, Zgavc T, et al. (2011) Serial semiquantitative imaging of brain damage using micro-SPECT and micro-CT after endothelin-1-induced transient focal cerebral ischemia in rats. Journal of nuclear medicine : official publication, Society of Nuclear Medicine 52:1987–1992.

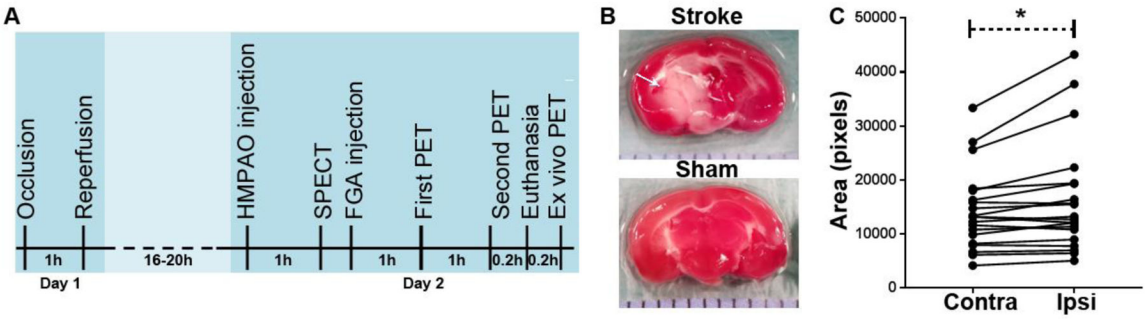

Figure 1:

Brain stroke model in mice. (A) Timeline of imaging where HMPAO and FGA imaging is done 1 day after stroke surgery. (B) Representative TTC-stained brain slices in stroke and sham mice. Stroke mice developed a large area of necrosis (arrow, white area) in the ipsilateral hemisphere. (C) Cerebral edema depicted by increase in area covered by ipsilateral hemisphere as compared to the contralateral hemisphere in 46 TTC-stained brain slices from 5 mice (*$p < 0.05$).

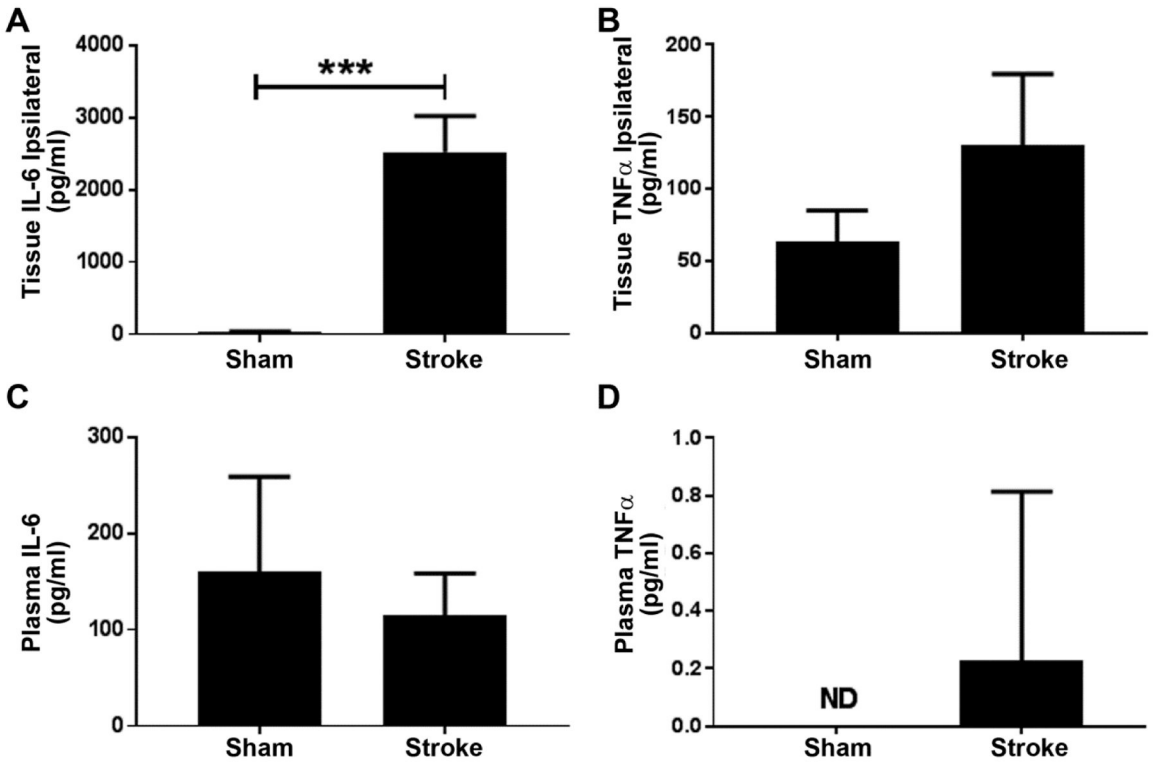

Figure 2:

Inflammatory markers in brain and plasma. (A) IL-6 levels in ipsilateral brain tissue (n = 6). (B) TNF-α levels in ipsilateral brain tissue (n = 6). (C) IL-6 levels in plasma (n = 9 from sham group and n = 8 from stroke group). (D) TNF-α levels in plasma. (*$p < 0.05$; ND= not detected; n = 3 each from sham and stroke groups).

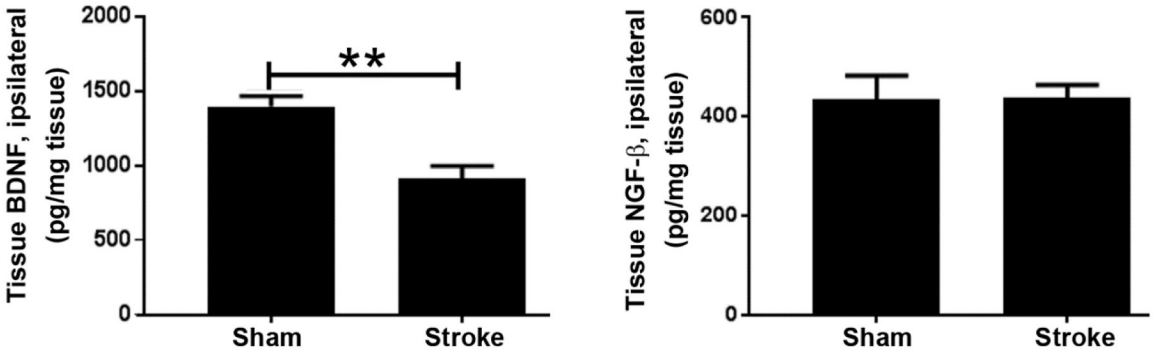

Figure 3:

Concentration of neurotrophin levels in the brain. (A) BDNF levels (n=5). (B) NGF-β levels (n = 5 from stroke group and n = 6 from sham group).

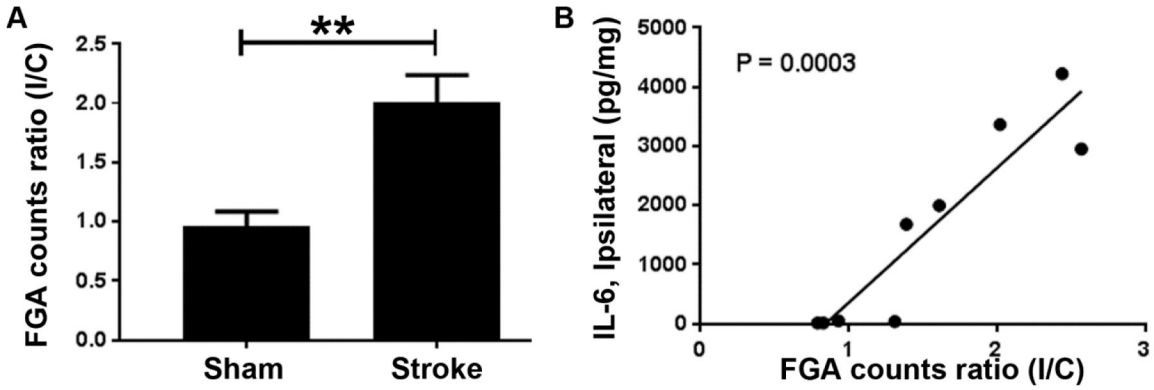

Figure 4:

Accumulation of FGA in the brain stroke. (A) Ipsilateral to contralateral ratio (I/C) of FGA counts in stroke mice (n = 5) is almost twice as high as in sham mice (n = 4). (B) Correlation of FGA I/C ratio with IL-6 levels in ipsilateral tissue (n = 4 from sham group and n = 5 from stroke group).

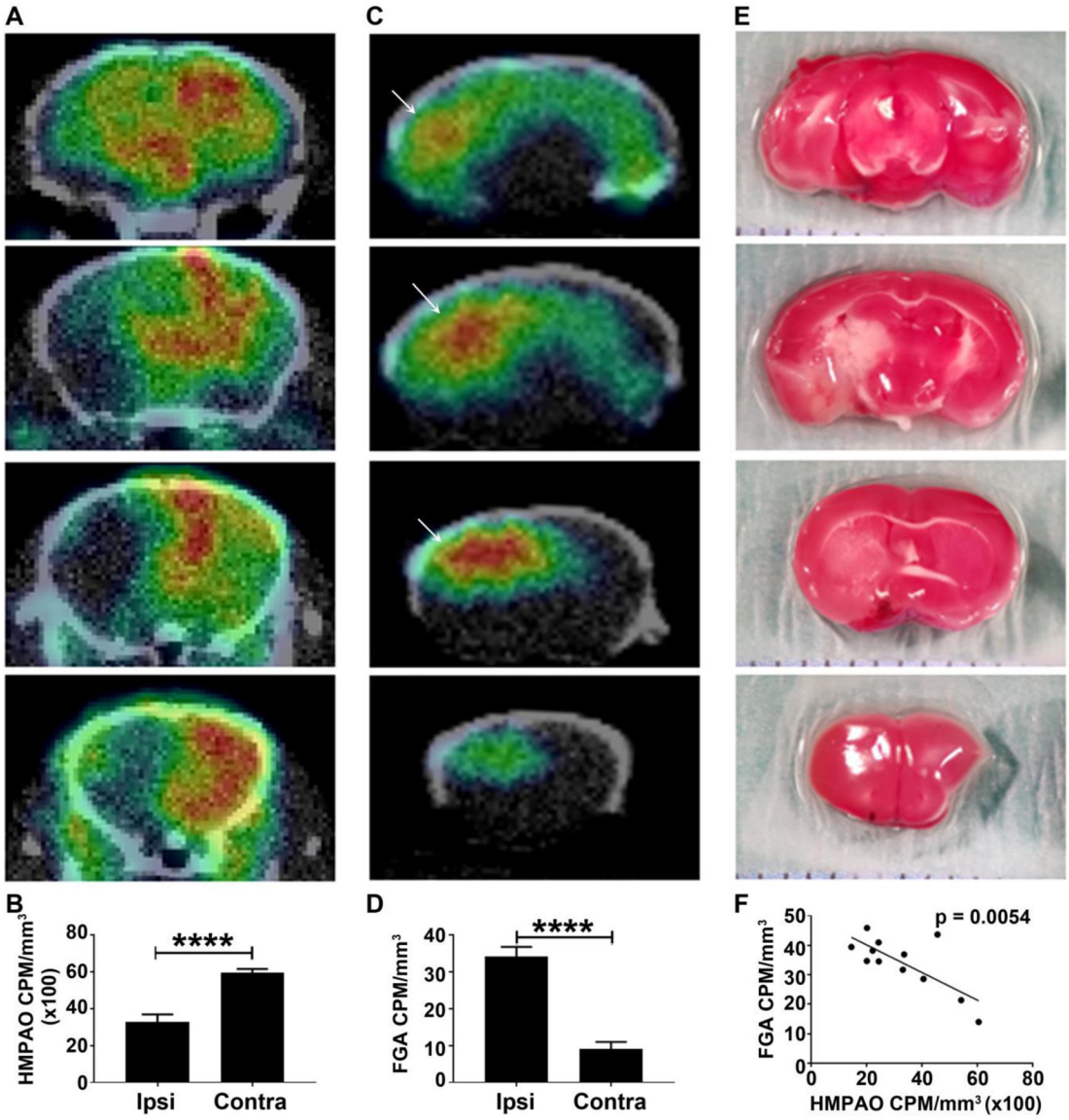

Figure 5:

Representative nuclear images of the brain stroke. (A) HMPAO/SPECT images showing perfusion deficit in ipsilateral hemisphere (n = 3). (B) Accumulation of HMPAO in ipsilateral versus contralateral hemisphere. (C) FGA/PET images showing necrotic region of the ipsilateral hemisphere (n = 3). (D) Accumulation of FGA in ipsilateral versus contralateral hemisphere. (E) TTC stained brain slices showing the area of necrosis (white region) primarily in the middle 2 slices of the brain Displayed images are coronal brain slices moving from the posterior (top row) to the anterior (bottom row) brain. (F) Correlation between FGA accrual and HMPAO accumulation in the ipsilateral hemisphere in mice with stroke (*$p < 0.05$).

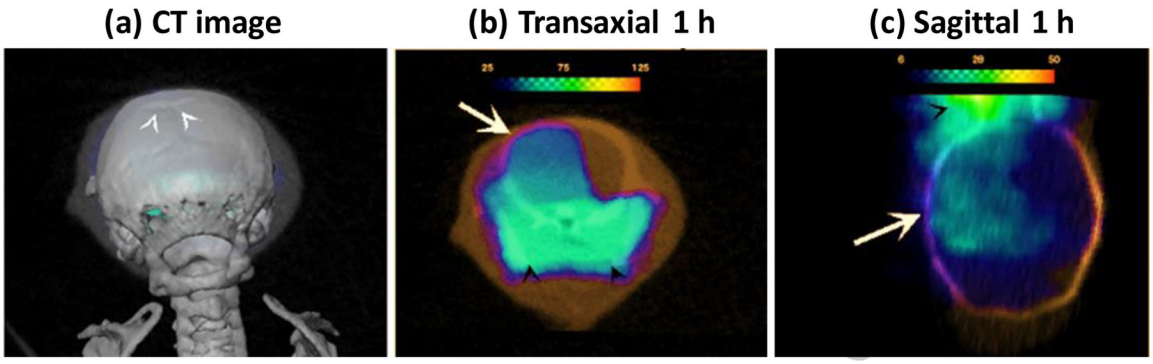

Figure 6:

FGA/PET images acquired within 3 h of stroke in mice model of t-MCAO. (A) Location of digital slicing in front of Bregma (white arrow heads) in super-imposed CT images is shown. (B-D) Views of FGA/PET images showing FGA accumulation in ipsilateral hemisphere (arrow) in mice with t-MCAO in left hemisphere. High level of sinus activity is also seen in the transaxial slices (black arrow heads).